Asian Journal of Pharmaceutical Sciences 20 (2025) 101022

Available online at www.sciencedirect.com

ScienceDirect

journal homepage: www.elsevier.com/locate/AJPS

Research Article

Enhancing temozolomide *in vivo* stability and efficacy through hybrid nanoconjugate approach for improved glioblastoma multiforme treatment

Prabhjeet Singh[a], *Deepak Kumar Sahel*[a], *Reena Jatyan*[a], *Kiran Bajaj*[b], *Anupama Mittal*[a], *Deepak Chitkara*[a,*]

[a] *Department of Pharmacy, Birla Institute of Technology and Science (BITS) Pilani, Pilani Campus, Pilani 333031, India*
[b] *Department of Chemistry, Amity Institute of Applied Science, Amity University, Noida Campus, Noida 201301, India*

ARTICLE INFO

Article history:
Received 13 November 2023
Revised 17 August 2024
Accepted 4 September 2024
Available online 23 January 2025

Keywords:
Hybrid nanoconjugates
Polymer-drug conjugate
Temozolomide delivery
Glioma
Brain delivery
Biocompatible hybrid carrier

ABSTRACT

Temozolomide (TMZ) is considered as a standard-of-care DNA alkylating agent for treating glioblastoma multiforme. Despite being a highly potent molecule, TMZ poses several limitations, including short half-life, rapid metabolism, low brain bioavailability and dose-dependent toxicities. Attempts have been made to improve the delivery of TMZ that mainly exhibited nominal therapeutic outcomes. In the current study, we have conjugated TMZ to mPEG-b-P(CB-{g-COOH}) copolymer to obtain mPEG-b-P(CB-{g-COOH; g-TMZ_n}) that demonstrated improvement in stability and efficacy. Further, a hybrid TMZ nanoconjugate formulation was developed using mPEG-b-P(CB-{g-COOH; g-TMZ_{40}}) and mPEG-polylactic acid (mPEG-PLA) showed an average size of 105.7 nm with narrow PDI of <0.2 and TMZ loading of 21.6 %. Stability was assessed under physiological conditions wherein TMZ was found to be stable with a half-life of ~194 h compared to 1.8 h for free TMZ. The Hybrid TMZ nanoconjugates showed improved intracellular uptake and reduced IC_{50} values in C6 and U87MG glioma cells. Furthermore, they exhibited better *in vivo* therapeutic outcome, *i.e.*, reduced brain weight, hemispherical width ratio and improved survival rate in C6-cell induced orthotropic glioma model in *Sprague Dawley* rats compared to the free TMZ-treated and positive control animals. Histopathological evaluation also revealed reduced cell infiltration in the lungs and reduced toxicity in major organs. Overall, the hybrid nanoconjugates of TMZ significantly improved its stability and efficacy in the GBM model, thereby opening newer avenues for treatment.

* Corresponding author. Department of Pharmacy, Birla Institute of Technology and Science (BITS) Pilani, Pilani Campus, Pilani 333031, India.
E-mail address: deepak.chitkara@pilani.bits-pilani.ac.in (D. Chitkara).
Peer review under responsibility of Shenyang Pharmaceutical University.

https://doi.org/10.1016/j.ajps.2025.101022

1. Introduction

Temozolomide (TMZ) is a second-generation DNA alkylating agent and used as a standard-of-care chemotherapeutic agent for the treatment of glioblastoma multiforme (GBM). TMZ is marketed as Temodal® in the form of capsules and injections, given *via*. oral and parenteral routes, respectively. Though a potent molecule, TMZ exhibits several limitations, such as short half-life (~1.8–2 h), rapid pH-dependent hydrolysis, and speedy clearance, resulting in lesser accumulation in the brain and dose-dependent toxicities. Hydrolysis of the molecule under physiological conditions results in the conversion of TMZ into its metabolite, MTIC (3-methyl-(triazen-1-yl)imidazole-4-carboxamide) and AIC (5-aminoimidazole-4-carboxamide), which cannot permeate into the cells effectively. Only <1 % of the dose reaches the brain intact, thereby rendering the drug with sub-therapeutic outcomes. In order to achieve the therapeutic effect, high doses of TMZ are given, resulting in dose-dependent hematological toxicities. Several approaches have been explored to overcome these limitations, including the encapsulation in nanocarriers of organic (lipids, polymers, dendrimers, etc.) and inorganic (silica, quantum dots, gold, silver, etc.) materials that showed improved TMZ delivery as well as preparation of conjugates with small molecules and polymers [1]. For instance, Nordling-David et al. prepared TMZ-loaded PEGylated liposomes using a thin film hydration method, yielding a small vesicle of 121 nm with an encapsulation efficiency of 23 % (w/w). *In vivo* assessment showed non-significant improvement in the survival rate compared to free TMZ [2]. Similarly, Duwa et al. prepared TMZ-loaded PLGA nanoparticles actively functionalized with cetuximab targeting EGFR receptors. Physiochemical characterization showed an average particle size of ~162 nm with a narrow PDI of 0.16 and encapsulation efficiency of 28.0 % at drug loading of 1.4 % (w/w) [3]. TMZ has a solubility of 5 mg/ml, posing challenges in encapsulating into the nanocarriers. To overcome, several derivatives of TMZ were synthesised with introduction of alkyl, allyl, methylene ester, amides, alcohols, propargyl, thioesters, sulfones and sulfoxides groups to TMZ molecule [4]. Likewise, TMZ has been conjugated with small molecules such as fatty acids, doxorubicin, γ-carbolines, 5-nitro-2-(3-phenylpropylamino)-benzoate (NPPB), perillyl alcohol, etc., and polymer including poly-(2-methacryloyloxyethyl phosphorylcholine) (MPC), poly(β-L-malic acid), poly(2-ethyl-2-oxazoline), etc [5–12]. TMZ conjugated to the polymeric backbone demonstrated improved drug loading capacity, systemic circulation, tissue targeting, ease in fabrication and better biocompatibility. Likewise, a series of polymer-TMZ conjugates depicted drug loading capacity up to 35 %–50 % (mol%) with improved stability half-life ranging from 2 to 19 folds compared to free TMZ. The *in vitro* cell-based assays also depicted marked enhancement in the cytotoxicity and uptake in glioma cells [9]. In another study, multifunctional targeted poly(β-L-malic acid) conjugated to TMZ was synthesized, resulting in particles of 6.5–14.8 nm, improved loading capacity up to 17 % (w/w) with enhanced stability of TMZ from 1.8 to 5–7 h [10]. We have previously reported the drug conjugates using PEG-polycarbonate, providing ample opportunity to attach the drug to the polycarbonate backbone with improved loading capacity, stability and efficacy [13]. Though conjugating TMZ with mPEG-polycarbonate overcome the limitations associated with TMZ, there is still a lot of scope for further improvement in the drug stability and delivery of the molecule. Combining biocompatible polymers with polymer-drug conjugates could provide benefits such as improved stability, biomimetic nature, drug accumulation to the target site, with reduced clearance and toxicity. Several other hybrid nanosystems have been explored earlier. For instance, polymer-lipid hybrid nanoparticles were prepared using PLGA polymer, and HSPC, DSPC and cholesterol as a lipid by the solvent emulsification method. The hybrid lipid-polymer nanosystem exhibited an average particle size of 256 nm with an encapsulation efficiency of >60 % at drug loading of ~3 % (w/w) [14]. Previously, we have reported polymer-lipid hybrid systems to deliver small molecules [15–17]. Combining the polymer-polymer-drug conjugates provides an ample opportunity to modify and improve the delivery system.

In the current research, we prepared a hybrid system comprised of polymer-TMZ conjugate and mPEG-PLA. Initially, a series of TMZ-polymer conjugates (mPEG-b-P(CB-{g-COOH; g-TMZ_n}) (wherein, $n = 20, 40$ and 60 TMZ units) were prepared and screened, wherein TMZ was covalently conjugated to the polycarbonate block polymer. The obtained conjugates were characterized using NMR and UV spectroscopy. Further, hybrid TMZ nanoconjugates were prepared and characterized for their *in vitro* and *in vivo* efficacy evaluation in the C6 cells-induced syngeneic orthotropic glioma model, wherein brain physiology, survival rate, change in body weight, tumor burden and organ toxicity were assessed.

2. Materials and methods

2.1. Materials

Temozolomide (TMZ, >98 %), tert–butyl carbazate, 1H-benzotriazol-1-yloxytripyrrolidinophosphonium hexafluorophosphate (PyBOP) and N,N-diisopropylethylamine (DIPEA) were purchased from TCI chemicals (Tokyo, Japan). Dulbecco's modified eagle medium (DMEM), minimum essential media (MEM), fetal bovine serum (FBS), SnakeSkin™ dialysis tubing (MWCO. 10 KDa), and Annexin-V ready flow conjugates kit were procured from ThermoFisher Scientific (Massachusetts, USA). Methoxy poly(ethylene glycol) (mPEG, 5 KDa), tin(II) 2-ethylhexanoate, DL-lactide, and propidium iodide (PI) were obtained from Sigma-Aldrich (St. Louis, USA). 1,4-dioxane and palladium on carbon (Pd/C) were purchased from Spectrochem (Mumbai, India). 3-(4,5-dimethylthiazol-2-yl)−2,5-diphenyltetrazolium bromide) (MTT), 1-(3-dimethylaminopropyl)−3-ethylcarbodiimide hydrochloride (EDC•HCl), and hydroxybenzotriazole (HOBT) were obtained from Sisco Research Laboratories (Mumbai, India). All other reagents and chemicals used were of analytical grade and bought from local vendors.

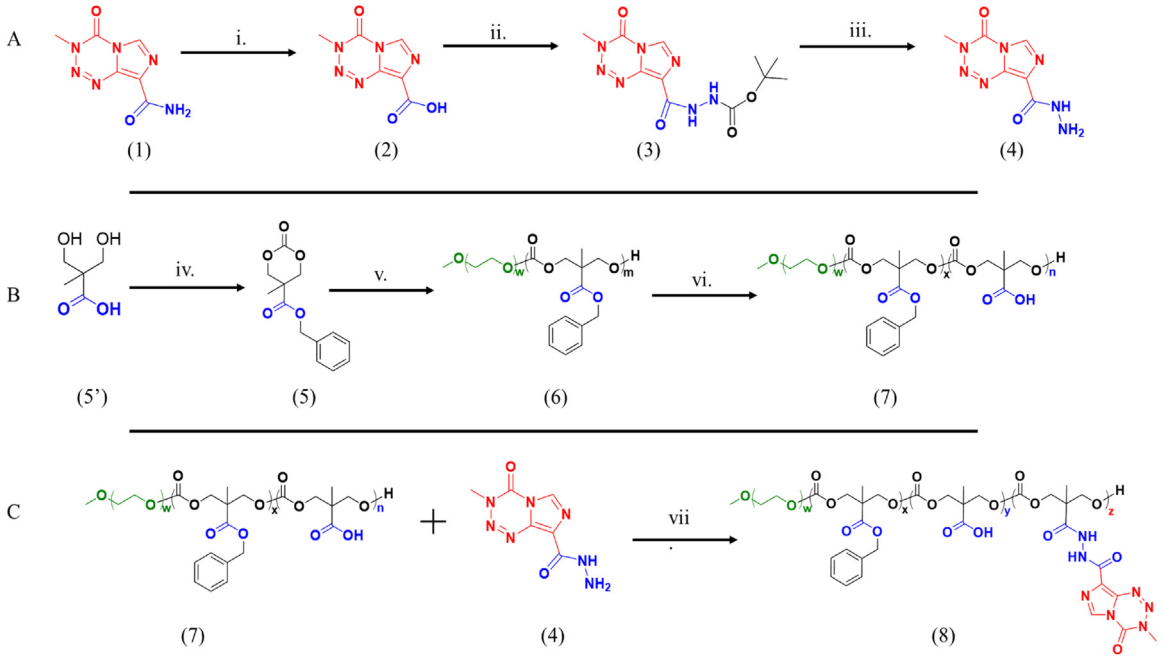

Fig. 1 – Reaction scheme for the synthesis of TMZ-polymer conjugates. (A) Synthesis of TMZ hydrazide: (i) $NaNO_2$, H_2SO_4, 4–8 °C, overnight, (ii) t–butyl carbazate, PyBOP, TEA, overnight, (iii) 1,4-dioxane•HCl, 4–6 h. (B) Synthesis of polycarbonate polymer with free COOH group: (iv) Benzyl bromide, KOH, 100 °C, overnight, then triphosgene, pyridine, acetone-dry ice bath, 4 h, (v) mPEG, tin(II)-ethylhexanoate, microwave-assisted ROP, 130 °C, 1 h, (vi) Pd/C, H_2, 5 h; (C) Synthesis of mPEG-b-P(CB-{g-COOH; g-TMZ_n}): (vii) EDC/HOBT coupling, DIPEA, N_2, 4–8 °C

2.2. *Synthesis of polymeric drug conjugate of TMZ (mPEG-b-P(CB-{g-COOH; g-TMZ_n}))*

A series of polymeric conjugates of TMZ were synthesized by reacting TMZ hydrazide derivative with amphiphilic mPEG-b-P(CB-{g-COOH}) copolymer. TMZ-hydrazide derivative was synthesized using a multistep reaction (Fig. 1). Initially, TMZ **(1)** was converted to TMZ acid **(2)** [10], then reacted with t–butyl carbazate to form Boc-protected TMZ hydrazide (TMZ-Boc) **(3)**, followed by cleavage of Boc using saturated dioxane·HCl to afford unprotected TMZ hydrazide (TMZ-H) **(4)** [8]. An amphiphilic copolymer, mPEG-b-P(CB-{g-COOH}), with free carboxyl pendant groups was synthesized in a multistep reaction, wherein 5-methyl-5-benzyloxycarbonyl-1,3-dioxane-2-one (MBC) **(5)** carbonate monomer was synthesized, as reported previously [18], followed by ring-opening polymerization (ROP) with mPEG as macroinitiator to yield mPEG-b-P(CB) **(6)** copolymer. The protective benzylic pendant was removed using catalytic hydrogenation to obtain the mPEG-b-P(CB-{g-COOH}) **(7)**. TMZ-H (4) was reacted to mPEG-b-P(CB-{g-COOH}) **(7)** polymer using EDC/HOBT coupling to obtain polymer conjugate of TMZ (mPEG-b-P(CB-{g-COOH; g-TMZ_n}) **(8)**. All reactions were carried out under a dry nitrogen atmosphere using the standard protocol as mentioned in supplementary materials. The synthesized intermediates, monomers, and polymers were thoroughly characterized using ^{1}H NMR (400 MHz) and ^{13}C NMR (101 MHz) spectra using Bruker AVANCE III 400 MHz NMR spectrometer (Massachusetts, USA) at 20 °C either using DMSO–d_6 or $CDCl_3$ with tetramethylsilane (TMS) as an internal reference. High-resolution mass (HRMS) spectra were recorded using Agilent Technologies 6545 Q-TOF LC/MS system (Agilent Technologies, Inc., California, USA) with electrospray ionization mode to detect the mass of monomers and their adducts. UV–visible spectra for synthesized compounds were recorded using a Jasco-V750 spectrophotometer (Tokyo, Japan) at room temperature with a path length of 1 cm over the 200–800 nm wavelength range.

2.3. *Synthesis of mPEG-PLA copolymer (9)*

mPEG-PLA **(9)** was synthesized using the previously described microwave-assisted ring opening polymerization (ROP) method [19]. Briefly, DL-lactide (0.535 g, 3.71 mmol) was polymerized with mPEG (0.465 g, 93 mmol) as a macroinitiator in the presence of tin(II) ethyl hexanoate as a catalyst at 130 °C for 1 h. After that, the crude copolymer was allowed to cool at room temperature, followed by purification by dissolving it in chloroform and precipitating in isopropyl alcohol and diethyl ether twice. The purified mPEG-PLA polymer was dried under a vacuum and analyzed using ^{1}HNMR spectroscopy.

2.4. *Development of hybrid TMZ NCs*

A hybrid TMZ nanoconjugate (Hybrid TMZ NCs) containing mPEG-b-P(CB-{g-COOH; g-TMZ_{40}}) **(8)** and mPEG-PLA **(9)** was developed using a thin film hydration method as reported earlier [20]. Briefly, 75 mg **(8)** and 25 mg **(9)** were dissolved in DCM and ethanol mixture (3:1, v/v) and transferred to a

round bottom flask (RBF), followed by the formation of a thin film by removal of organic solvent using rotary evaporator. The RBF with a thin film was purged with dried nitrogen gas for 60 min. After that, the thin film was redispersed slowly using a phosphate-buffered saline (PBS, 10 mM) dispersive medium to yield a dispersion mixture. The dispersion was probe sonicated for 20 s at 20% amplitude under ice-cold condition, followed by centrifugation at 12,000 rpm for 10 min. TMZ stability and colloidal stability of Hybrid TMZ NCs were evaluated. The loading amount of TMZ was calculated from the weight ratio method using the simple UV–Vis spectrophotometer (λ_{max} 328 nm) and calculated as per the below-mentioned formulae:

$$\text{TMZ loading in (8) (\%)} = \frac{\text{Amount of TMZ present}}{\text{Amount of (8)taken}} \times 100\%$$

$$\text{TMZ loading in Hybrid nanoconjugate (\%)} = \frac{Amount\ of\ TMZ\ in\ (8)}{Total\ polymer\ (8\ \&\ 9)} \times 100\%$$

The hydrodynamic diameter, particle size (PS), polydispersity index (PDI) and surface zeta potential (ZP, ζ) were measured using dynamic light scattering (DLS) (Zetasizer Nano ZS, Malvern Panalytical Ltd, UK) at a measuring angle of 173° The surface morphology was evaluated by prior surface coating of Hybrid TMZ NCs with gold/chromium target for 120 s using Q150TES sputter coater, Quorum Technologies (Lewes, UK). After that, the coated particles were evaluated using Field Emission-Scanning Electron Microscopy (FE-SEM) (FEI, Apreo S LoVac, Thermo Fisher Scientific, MA, USA) with a spot size of 9 mm under vacuum.

2.5. Stability studies

The stability studies of the developed Hybrid TMZ NCs were performed under physiological pH at 4 °C and 37 °C. The samples were kept in a closed vial and incubated for specific period of time, followed by determination of changes in PS and TMZ remaining in the Hybrid TMZ NCs using DLS and UV method, respectively. For the DLS measurements, Hybrid TMZ NCs were taken at a concentration of 3 mg/ml and analyzed for the change in PS and PDI for 7 d Furthermore, the same samples were used to determine the TMZ remaining in the conjugates. For the UV stability analysis, the samples (free TMZ, free TMZ-H, mPEG-b-P(CB-{g-COOH; g-TMZ_{40}}), and Hybrid TMZ NCs) were taken and analyzed at predetermined time points (0, 6, 12, 24, 48, 72, 96 and 120 h) using UV–Vis spectrophotometry. The samples analyzed were withdrawn from the stock and diluted, and UV absorbance was evaluated at 328 nm for the TMZ remaining, and the stability graph of TMZ remaining was plotted over time.

2.6. Cell culture studies

C6 and U87MG glioma cell lines were obtained from the National Centre for Cell Sciences (NCCS, Pune, India), and were maintained in Dulbecco's Modified Eagle Medium (DMEM) and Minimum Essential Medium (MEM), respectively, supplemented with 10% fetal bovine serum (FBS) and 1% penicillin/streptomycin mixture, kept in an incubator at 37 °C with 5% CO_2. The cells were allowed to proliferate until 70%–80% confluency was achieved for further experimentation.

2.7. Cell viability assay

C6 and U87MG glioma cells were trypsinized and seeded in a 96-well cell-culture plate at a density of 5,000 cells/well, and incubated at 37 °C/ 5% CO_2 for 24 h. The following day, cells were treated with free TMZ or Hybrid TMZ NCs in a concentration range of TMZ equivalent to 100–1,500 μM and 25–1,000 μM for C6 and U87MG cells, respectively. After 72 h of treatment, media was replaced with fresh media containing 5 mg/ml MTT and kept for 4 h in an incubator. After the formation of formazan crystals, the media was discarded, and 200 μl DMSO was added to each well to dissolve the crystals. The extent of metabolic activity was measured by determining the absorbance at 570 nm and 630 nm using an Epoch microplate spectrophotometer (Biotek Instruments, USA). The cell viability was calculated using the below-mentioned equation [15]. Where, *As* is absorbance of sample wells; *Ac* is absorbance of control wells.

$$\text{Cell Viability (\%)} = \left\{ \frac{[\text{As}(570\ nm) - \text{As}(630\ nm)]}{[\text{Ac}\ (570\ nm) - \text{Ac}\ (630\ nm)]} \right\} \times 100\%$$

2.8. Apoptosis assay

Apoptosis analysis of Hybrid TMZ NCs was determined using the Annexin-V/PI-kit-based flow cytometry assay. Briefly, C6 and U87MG glioma cells were seeded in a 6-well plate (1×10^5 cells/well). The cells were incubated overnight, followed by the treatment with free TMZ and Hybrid TMZ NCs for 24 h. Thereafter, cells were washed with PBS, trypsinized, centrifuged, resuspended in 1× annexin binding buffer, and stained with Annexin-V/ PI in a dark condition for 15 min. Flow cytometry (Beckman Coulter, USA) was used to analyze the apoptosis rate and data was interpreted using CytExpert V3.0 software [15].

2.9. Cell uptake and endo-lysosomal assay

The cellular uptake of Hybrid TMZ NCs was determined using qualitative and quantitative methods. Briefly, cells (C6 and U87MG) were seeded in a 6-well plate (1×10^5 cells/well) and allowed to adhere for 24 h. Thereafter, the cells were treated with free coumarin-6 dye and coumarin-6-loaded Hybrid TMZ NCs, and incubated for 4 h. Subsequently, the cells were washed with PBS, fixed with 2% paraformaldehyde for 10 min, and counterstained with DAPI for 10 min to stain the nucleus. For qualitative analysis, fixed cells were observed under a fluorescence microscope (ZEISS, Germany), and respective microscopic images (DIC, DAPI, coumarin-6/FITC, and Overlay) were acquired for the treatment groups. The obtained data were interpreted using Zen Blue software V3.4. For quantitative analysis, the samples were trypsinized, washed with PBS, and evaluated for the quantitative uptake of coumarin-6-dye in glioma cells using the flow cytometry,

and the obtained data was interpreted using CytExpert V3.0 software as reported earlier [15].

In vitro lysosomal fate of the nanoparticles was investigated using coumarin-6 and LysoTracker™ Red DND-99 as a fluorescent probe. Briefly, the glioma cells (C6 and U87MG) were seeded in a 6-well plate (1×10^5 cells/well) and allowed to adhere for 24 h. On the following day, the cells were treated with coumarin-6 loaded Hybrid TMZ NCs for 4 h. After the treatment, media was discarded, and the cells were washed thrice with PBS, then incubated with LysoTracker™ Red DND-99 (1 μM) for 20 min, and fixed with 2% paraformaldehyde for 10 min and counterstained with DAPI for 10 min to stain the nucleus. The cells were observed under the confocal fluorescence microscope, and microscopic images (DAPI, coumarin-6/FITC, LysoTracker™ and Overlay) were acquired for the respective groups. The data was interpreted, and the colocalization index was determined using Zen software V3.4 [19].

2.10. C6 cells induced orthotropic glioblastoma model development in rats

C6 glioma cells were incubated until 70% of confluency, and cells were trypsinized with (0.25% trypsin/EDTA solution), washed with DMEM medium, and suspended in 80 μl sterile PBS. *Sprague Dawley* male rats, 6–8 week old, were used after the approval from the Institutional Animal Ethics Committee (IAEC) of BITS Pilani, with protocol no: IAEC/RES/23/08/Rev-3/32/26, and all the animal experiments were performed as per the Committee for the Purpose of Control and Supervision of Experiments on Animals (CPCSEA) guidelines. The rats were anesthetized with ketamine (90 mg/kg i.p.) and xylazine (9 mg/kg i.p.) for C6 glioma cells implantation. They were placed on the stereotaxic apparatus, and their heads were shaved before making a small incision of 3 cm to expose the skull. A 1 mm burr hole was drilled, and C6 cells (2×10^6) were injected at 2 mm anterior, 3 mm lateral and 4 mm depth to the bregma at a flow rate of 3 μl/min using Hamilton's syringe. After injection, the needle was kept in the same position additionally for 2 min to avoid backflow. After that, the burr hole was sealed using biodegradable wax, and the incision was closed with suture. The animal were placed back in their home cages and observed until they regained consciousness. Daily observation included, monitoring change in neurological behaviour, body weight, and right eye bulging as an indicator of tumor development.

2.11. In vivo efficacy studies

Briefly, C6 glioma cells-bearing rats were randomly taken and kept for 9 d The treatment phase started on Day 10 with treatment groups ($n = 5$) including, negative control, positive control, free TMZ, and Hybrid TMZ NCs. All drug treatments were given at a dose equivalent to 10 mg/kg of TMZ thrice a week for next 30 d The animals were regularly monitored for their change in body weight, locomotion and neurobehavioral activity. On Day 40 (30 d after treatment), animals were sacrificed, and major organs (heart, lungs, liver, spleen, kidney, etc.) were excised for histopathological evaluation. In addition, the excised brains of all the animals were isolated and evaluated for physical appearance, brain weight, hemispherical width ratio (RH/LH) and histopathological evaluation.

2.12. Statistical analysis

Results are expressed as mean ± SD or mean ± SEM. All the obtained data were analyzed using ANOVA (analysis of variance) followed by Tukey's test for comparison between treatment groups. $P < 0.05$ was considered statistically significant.

3. Results and discussion

3.1. Characterisation of mPEG-b-P(CB-{g-COOH; g-TMZ$_n$})

A series of TMZ-conjugated amphiphilic copolymers (*mPEG-b-P(CB-{g-COOH; g-TMZ$_n$}*) were synthesized in a multistep reaction, as shown in Fig. 1. Initially, free -NH_2 group of TMZ **(1)** was converted to TMZ-A **(2)** with free -COOH group to yield white precipitate (~91% yield) and characterized. Fig. S1 showed ^{1}H NMR (400 MHz, DMSO–*d6*) of TMZ-A showed peaks corresponding to δ 8.79 (s, 1H) and 3.87 (s, 3H). Further, the disappearance of two protons of -CON$\underline{H}_2$ of TMZ at δ 7.68–7.81 confirms the conversion of free -$CONH_2$ to the COOH group. ^{13}C NMR, ESI-TOF and HPLC chromatogram showed the successful conversion of TMZ to TMZ-A (Fig. S1-S3). The free -COOH of TMZ-A was protected with *t*–butyl carbazate to yield TMZ-Boc **(3)** using PyBOP coupling reagent. The crude product obtained was purified using column chromatography to yield a pure light-yellow solid (~62.1% yield). Fig. S1 showed ^{1}H NMR (400 MHz, $CDCl_3$) of TMZ-Boc with peaks at δ 9.08 (s, 1H), 8.36 (s, 1H), 7.13 (s, 1H), 3.95 (s, 3H) and 1.40 (s, 9H). ^{13}C NMR, ESI-TOF and HPLC showed the conversion of TMZ-A to TMZ-BOC (Fig. S1-S3). Subsequently, the deprotection of the Boc group was done using dioxane saturated with HCl, followed by washing with diethyl ether to obtain white powder (~65% yield). Fig. S1 showed ^{1}H NMR (400 MHz, DMSO–*d6*) of TMZ-H **(4)** with peaks at δ 8.95 (s, 1H), 3.89 (s, 3H), with the disappearance of 9 protons from TMZ-Boc. ^{13}C NMR, ESI-TOF and HPLC chromatogram and UV spectroscopy data showing its absorption maxima at 328 nm (Fig. 2 and S1-S3), signifying the integrity of TMZ after the synthesis of its hydrazine derivative.

In the phase B, cyclic monomer MBC was synthesized and characterized using ^{1}H NMR and ESI-TOF. Fig. S4 shows ^{1}H NMR (400 MHz, $CDCl_3$) of MBC with peaks at δ 7.36 (s, 5H), 5.22 (s, 2H), 4.70 (d, J = 10.9 Hz, 2H), 4.20 (d, J = 10.9 Hz, 2H), 1.33 (s, 3H) and ^{13}C NMR (101 MHz, $CDCl_3$) with peaks at δ 171.03, 147.54, 134.85, 128.86, 128.30, 73.03, 67.99, 40.31 and 17.63. $[M + H]^+$ ion peak at m/z 251.0909 da ($C_{13}H_{14}O_5$; cal. $[M + H]^+ = 251.0875$ da) indicates successful synthesis of MBC. Microwave-assisted ROP of MBC was initiated in the presence of mPEG as macroinitiator and tin(II) ethyl hexanoate as a catalyst to obtain mPEG-b-P(CB) **(6)** with a yield of 70%. Fig. S5 shows ^{1}H NMR (400 MHz, $CDCl_3$) characteristic peak at δ 7.37 – 7.26 ($C_6\underline{H}_5$), δ5.18 – 5.07 ($C\underline{H}_2$-Bn), δ4.35 – 4.19 ($C\underline{H}_2$-O-*bis*MPA), δ3.64 ($C\underline{H}_2$ of PEG), δ3.38 ($C\underline{H}_3$-O-PEG), δ1.28 – 1.16 (-$C\underline{H}_3$ of bisMPA) and ^{13}C NMR (101 MHz, $CDCl_3$)

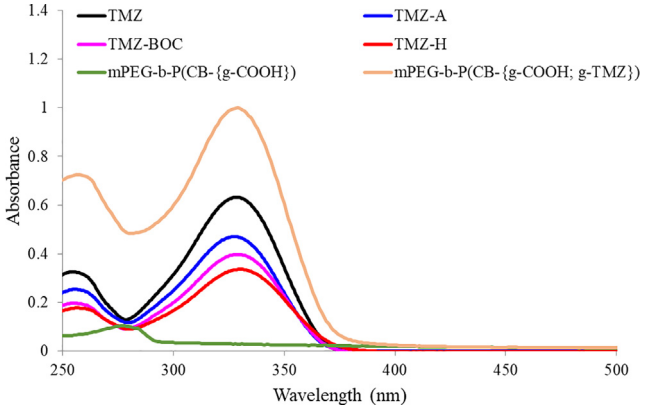

Fig. 2 – Characterization of TMZ and its derivatives using UV–Vis spectroscopy.

showed peaks at δ172.00, 154.44, 135.47, 128.68, 128.49, 128.44, 128.09, 70.68, 68.70, 67.16, 46.66 and 17.51. The protective benzylic groups of mPEG-b-P(CB) were removed using catalytic hydrogenation in the presence of Pd/C to obtain mPEG-b-P(CB-{g-COOH}) **(7)** with the free carboxylic pendant group on the polymer backbone (~60 % yield). Fig. 3A shows ^{1}H NMR (400 MHz, DMSO–d6) peak at δ 13.6–12.8 (-COOH), 4.22–4.11 (CH_2-O-*bisMPA*), 3.50 (-CH_2 of PEG), 3.23 (CH_3-O-PEG), 1.13 (-CH_3 of *bisMPA*) and reduction in the number of bulky benzylic protons at δ 7.33 (-C_6H_5) and 5.13 (CH_2-Bn). ^{13}C NMR (101 MHz, DMSO–*d6*) showed peaks at δ 176.62, 175.07, 173.51, 154.20, 153.97, 151.47, 139.18, 128.43, 128.04, 127.55, 124.92, 71.30, 69.81, 68.88, 67.03, 63.86, 63.58, 49.48, 47.48, 45.67, 34.39, 30.44, 25.14, 21.04 and 16.94 (Fig. S6A). Carbodiimide coupling chemistry was utilized for grafting the hydrazine derivative of TMZ (TMZ-H) to the free carboxylic pendent of the polycarbonate polymer backbone of (**7**) to yield the series of mPEG-b-P(CB-{g-COOH; g-TMZ$_n$}) **(8)**. Fig. 3B shows ^{1}H NMR (400 MHz, DMSO–*d6*) peaks at δ 10.31(-NH–NH-), 10.05 (-NH–NH-), 8.84 (N–CH=N- of TMZ), 7.32 (-C_6H_5 of MBC), 5.13 (CH_2-Bn), 4.19 (CH_2-O-*bisMPA*), 3.87 (N–CH_3 of TMZ), 3.51 (-CH_2 of PEG), 3.16 (CH_3-O-PEG), 1.11 (-CH_3 of *bisMPA*), indicating

Table 1 – Loading capacity of nanoconjugates

Formulation	Loading efficiency (% w/w)
TMZ	n.a.
TMZH	n.a.
mPEG-b-P(CB-{g-COOH; g-TMZ$_{20}$})	16.8 %
mPEG-b-P(CB-{g-COOH; g-TMZ$_{40}$})	28.7 %
mPEG-b-P(CB-{g-COOH; g-TMZ$_{60}$})	37.99 %
Hybrid TMZ NCs[a]	21.6 %

[a] mPEG-b-P(CB-{g-COOH; g-TMZ$_{40}$} and mPEG-PLA.

the synthesis of mPEG-b-P(CB-{g-COOH; g-TMZ$_{40}$}). ^{13}C NMR (101 MHz, DMSO–*d6*) showed peaks at δ 197.08, 173.81, 173.75, 173.70, 158.80, 154.12, 147.56, 139.13, 135.13, 128.76, 88.25, 74.13, 73.94, 69.80, 69.06, 45.70, 45.29, 36.23, 17.16 and 15.66 (Fig. S6B). The above-synthesized polymer-TMZ conjugates were characterized based on TMZ units attached equivalent to 20, 40 and 60 units grafted to the polymer backbone **(7)**. The obtained mPEG-b-P(CB-{g-COOH; g-TMZ$_n$}) conjugates depicted the loading efficiency of 16.8 %, 28.82 % and 37.99 % (w/w) for 20, 40 and 60 units of TMZ units, respectively, and their loading capacities are represented in Table 1.

3.2. *Characterization of mPEG-b-P(CB-{g-COOH; g-TMZ$_n$}) NPs and mPEG-PLA*

The obtained mPEG-b-P(CB-{g-COOH; g-TMZ$_{20}$}), mPEG-b-P(CB-{g-COOH; g-TMZ$_{40}$}) and mPEG-b-P(CB-{g-COOH; g-TMZ$_{60}$}) were initially screened based on the PS and surface morphology using DLS and SEM, respectively. The nanoconjugates of TMZ were prepared in various dispersive mediums (including pH 5.0, 6.0 and 7.4) and demonstrated varying particle sizes based on the units of TMZ units attached. mPEG-b-P(CB-{g-COOH; g-TMZ$_{20}$}) demonstrated size ranging from 237.1 to 323.7 nm with loading capacity of 16.8 % (w/w), mPEG-b-P(CB-{g-COOH; g-TMZ$_{40}$}) showed an average particle size ranging from 90.9 to 207.2 nm with loading capacity of 28.7 % (w/w), while, mPEG-b-P(CB-{g-COOH; g-TMZ$_{60}$}) exhibited an average particle size from

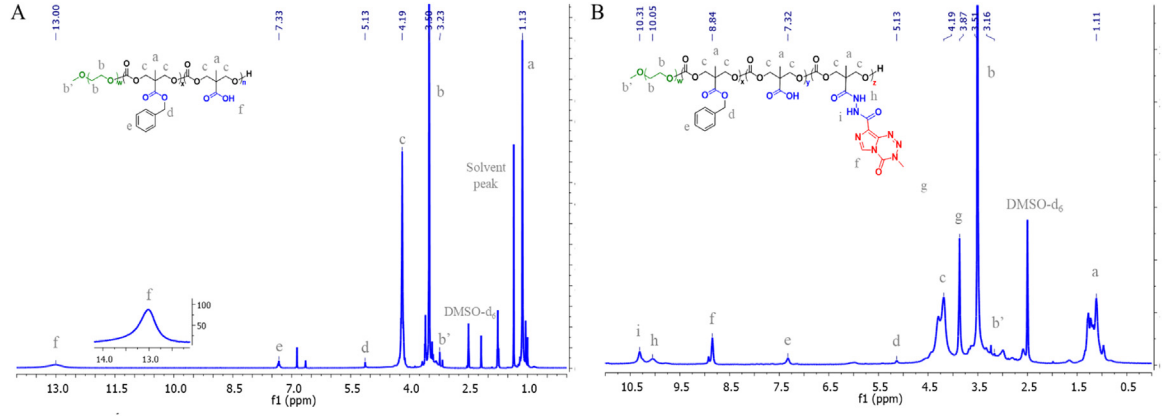

Fig. 3 – ^{1}HNMR spectrum of (A) polycarbonate polymer with free COOH group (mPEG-b-P(CB-{g-COOH}), and (B) TMZ-polymer conjugate (mPEG-b-P(CB-{g-COOH; g-TMZ$_{40}$}).

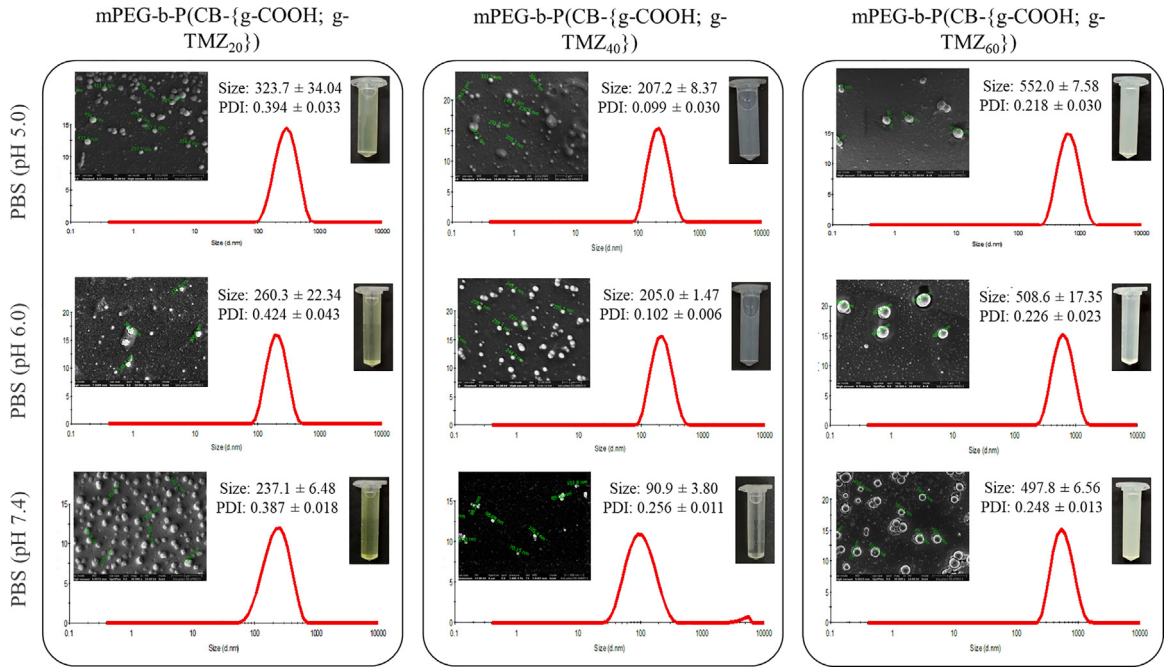

Fig. 4 – Characterization of TMZ-polymer conjugates mPEG-b-P(CB-{g-COOH; g-TMZ$_n$}) in various dispersive mediums (PBS 10 mM: pH 5.0, pH 6.0, pH 7.4) using DLS, SEM images and their pictogram.

497.8 to 552 nm with loading capacity of 37.99 % (w/w) (Fig. 4). Although the nanoconjugates in various dispersive medium showed a good TMZ loading capacity of up to 37.99 % w/w, the size obtained using mPEG-b-P(CB-{g-COOH; g-TMZ$_{60}$}) was not suitable for the *in vitro* and *in vivo* therapeutic application. Furthermore, mPEG-b-P(CB-{g-COOH; g-TMZ$_{20}$}) was excluded from the further studies as the loading capacity was significantly less, *i.e.*, 16.8 % (w/w) with an average PS higher than 200 nm. Interestingly, mPEG-b-P(CB-{g-COOH; g-TMZ$_{40}$}) with 40 TMZ units with a loading capacity of 28.7 % (w/w) depicted pH dependent change in PS of 207.2, 205 and 90.9 ± 3.80 nm under pH 5.0, 6.0 and 7.4, respectively, and zeta potential of −12.06 ± 0.86 mV (at pH 7.4), which could be used as a potential nanoconjugate with optimal size and improved loading capacity (Figs. 4 and 5 and Table 1). The significant reduction in PS to 90.9 nm in pH 7.4 was observed in mPEG-b-P(CB-{g-COOH; g-TMZ$_{40}$}); wherein, several free COOH functional groups remained in free form post conjugation of TMZ derivative to the amphiphilic copolymer (mPEG-b-P(CB-{g-COOH}). It is very well known that free COOH groups remain as unionized under acidic conditions (pH <7.0), while under alkaline conditions (pH >7.0), it gets ionized and form free -COO$^-$ ion, rendering the backbone towards more polar [21], resulting in lesser particle size. This could be attributed due to the appropriate hydrophilic to lipophilic balance of the TMZ-polymer conjugate, wherein a balance between the units of attached TMZ and free COOH groups was observed in such a way that exhibited the lowest size compared to the other conjugates. Overall, the above synthesized nanoconjugates exhibited pH dependent change in particle size *i.e.*, the size of nanoparticles was found to reduce as the pH increased from pH 5.0 to pH 7.4 (Fig. 4). Similarly, Li et al. observed the increase in particle size as the pH of dispersive medium was reduced from pH 7.4 to 5.5 using folate functionalized soybean phosphatidylcholine complex-loaded PEG-lipid-PLA hybrid nanoparticles, showing the role of pH in the modulation of particle size of the nanocarrier system [22]. ^{1}H NMR (400 MHz, $CDCl_3$) of mPEG-PLA **(9)** indicates an average molecular weight of 10 KDa with ~70 units of lactic acid.

3.3. *Characterization of Hybrid TMZ NCs*

Hybrid TMZ NCs consisting of mPEG-b-P(CB-{g-COOH; g-TMZ$_{40}$}) **(8)** and mPEG-PLA **(9)** (3:1 ratio) were prepared using the thin film hydration method. The resulting Hybrid TMZ NCs depicted PS of 105.7 ± 0.99 nm with a narrow PDI of 0.106 ± 0.033 and a surface zeta potential of ζ: −6.79 ± 1.61 mV (Fig. 5). The SEM images confirmed the particles obtained were uniform in size and spherical in morphology. The loading capacity of the Hybrid TMZ NCs was found to be ~21.6 % (w/w) (Table 1). In previous reports, Xu et al. prepared a series of poly(2-ethyl-2-oxazoline) (PEtOz) conjugated TMZ (PEtOz-TMZ), exhibiting the drug loading capacity ranging from 2.2 % to 4.1 % (w/w) [11]. In another report, Patil et al. prepared TMZ conjugated multifunctional poly(β-L-malic acid) platform, resulting in the polymer TMZ conjugates with drug loading up to 17 % (w/w) against the glioma cells [10].

3.4. *Stability of Hybrid TMZ NCs*

The stability of nanoconjugates in the biological environment is an important aspect that can impact the therapeutic outcome. The colloidal stability of the Hybrid TMZ NCs was determined in physiological pH at 4 °C and 37 °C for up to 7 d At 4 °C, mPEG-b-P(CB-{g-COOH; g-TMZ$_{40}$}) and Hybrid TMZ NCs showed no significant change in PS for 7 d At 37 °C, mPEG-

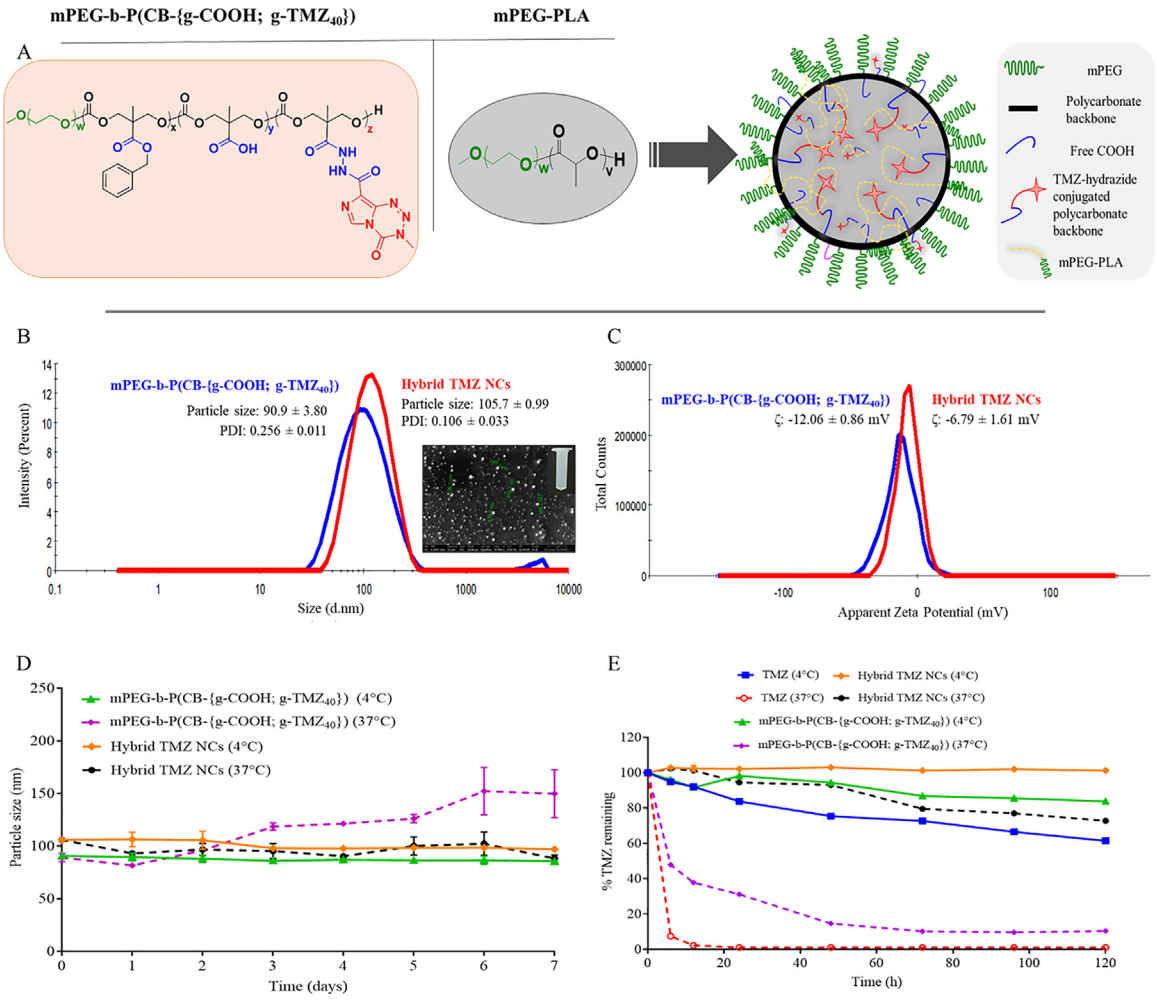

Fig. 5 – Characterization of hybrid nanoconjugates. (A) Schematic representation of hybrid nanoconjugates in combination with mPEG-b-P(CB-{g-COOH; g-TMZ$_{40}$}) and mPEG-PLA, (B) particle size with SEM image and pictograph, (C) surface zeta potential, D) DLS-based colloidal stability, and (E) UV-based TMZ stability evaluation of Hybrid TMZ NCs in PBS (pH 7.4) at 4 °C and 37 °C.

b-P(CB-{g-COOH; g-TMZ$_{40}$}) demonstrated a marked change in PS after 2 d, while Hybrid TMZ NCs were stable for over 7 d TMZ exhibits hydrolytic degradation to form MTIC and AIC under physiological pH with a half-life of 1.8 h. The Hybrid TMZ NCs degradation behaviour was determined (Fig. 5) for 120 h and compared with free TMZ and mPEG-b-P(CB-{g-COOH; g- TMZ$_{40}$}). The conjugation of TMZ in *mPEG-b-P(CB-{g-COOH;* g-TMZ$_{40}$}) has improved the half-life to 5.88 h, but it is still not significantly stable for the *in vivo* application. Surprisingly, the TMZ stability of the Hybrid TMZ NCs was significantly improved for over 120 h with half-life improved from 5.88 h to ~194 h at physiological conditions (pH 7.4, 37 °C) (Fig. 5). This observation could be attributed due to the formation of hybrid nanosystem that protects the susceptible TMZ molecule within the nanoassembly, eventually rendering the degradation process slower. Literature evidence also suggested that hybrid system can provide advantages such as improved drug stability, colloidal stability, biocompatibility, combinational drug delivery, ease in fabrication, controlled release properties, and reduced toxicities [23]. For instance, Tahir *et al.* prepared lipid-polymer hybrid nanoparticles using PLGA polymer and DSPE-PEG lipid, yielding particle size ranging from 173 to 208 nm with excellent physical stability, biocompatibility, and a higher degree of internalization compared to free drug [24]. Similarly, Ebrahimian et al. prepared lipopolymeric nanoparticles using PLGA and PLGA-PC to enhance the stability of bromelain and facilitate oral delivery. The hybrid system showed stable nanoparticles with no significant change in PS, PDI and ZP for over 1 month of storage [25].

Though a slow degradation kinetics is expected that may impact the therapeutic effect, however the results of *in vitro* and *in vivo* evaluation could demonstrate improved pharmacological response in treating glioma. Besides, the anti-GBM outcome could be observed as these Hybrid TMZ NCs could accumulate in the tumor microenvironment due to the EPR (enhanced permeation and retention) effect. The presence of the leaky vascular fenestrations makes the nanoparticles of <300 nm in range show enhanced permeation across the BBB/BBTB and the damaged

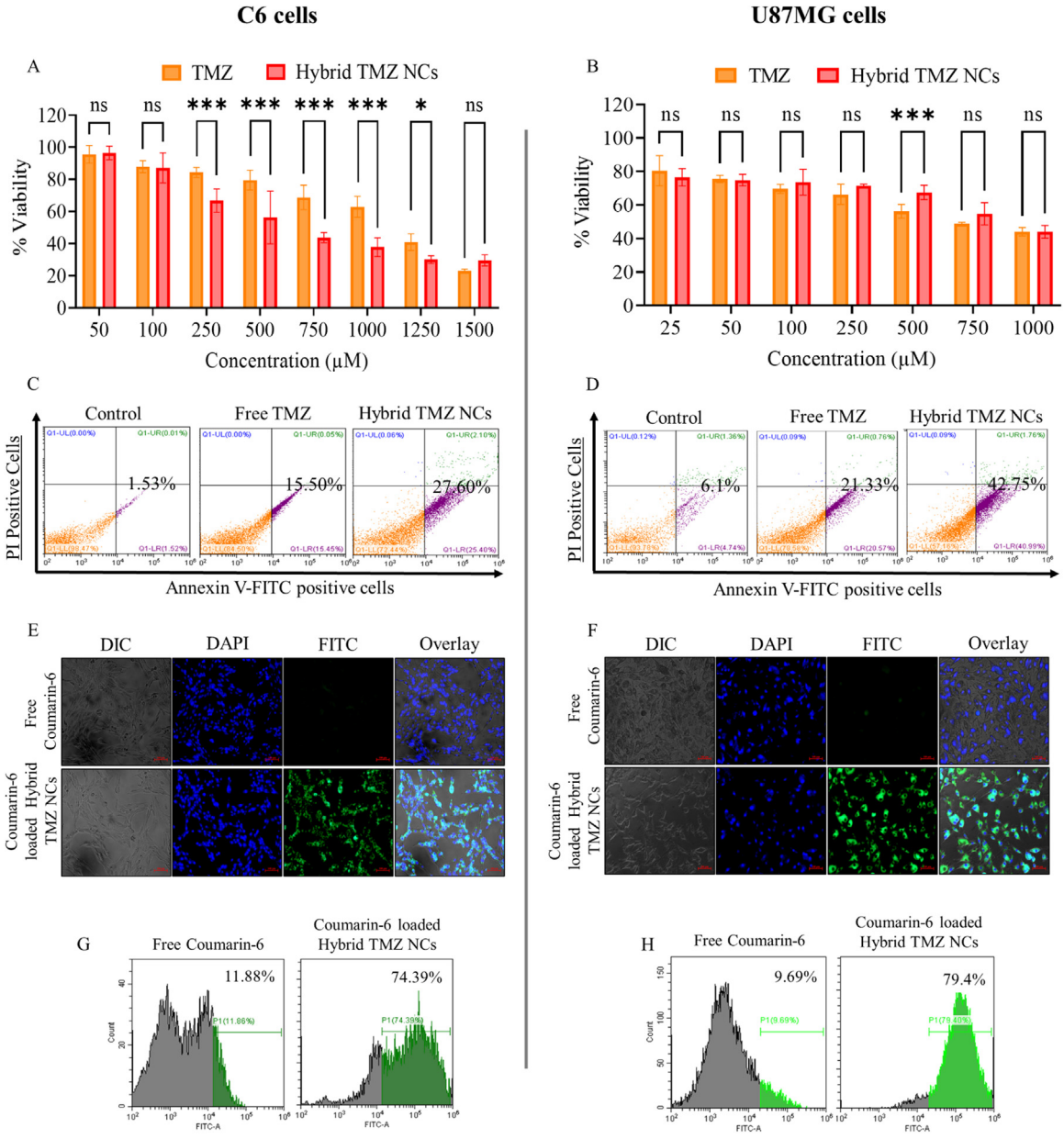

Fig. 6 – *In vitro* cell-based evaluation of Hybrid TMZ NCs in glioma cells. Cell cytotoxicity using MTT assay in (A) C6 and (B) U87MG glioma cells. Annexin-V/PI-based apoptosis assay in (C) C6 and (D) U87MG glioma cells. Coumarin-6-based cellular uptake assay. (E & F) Qualitative evaluation using microscopy in C6 and U87MG glioma cells, (G & H) Quantitative uptake using flow cytometry in C6 and U87MG glioma cells, respectively.

glymphatic drainage system, resulting in an increase in nanoparticle concentration nearby tumor region. Further, we hypothesize that conjugated TMZ could directly release the methyl diazonium ion at pH 7.4, which acts as an electrophile and causes methylation to susceptible sites of DNA, especially at O^6-methylguanine (O^6-MG), N^7-methylguanine (N^7-MG), and N^3-methyladenine (N^3-MA), resulting in mismatching of base pairs and DNA double-strand break, causing cell cycle arrest and eventually cell death. Overall, *in vitro* evaluation of the nanoconjugates has demonstrated the marked enhancement of the physiochemical properties of the TMZ, wherein the stability and loading capacity of the TMZ were significantly improved using the above approach.

3.5. *In vitro uptake, endo-lysosomal fate and cytotoxicity of hybrid TMZ NCs*

The cell viability profiles of treatment groups (including free TMZ and Hybrid TMZ NCs) were determined in C6 and U87MG glioma cell lines, as shown in Fig. 6. The Hybrid TMZ NCs significantly improved IC_{50} to ~645 μM compared to ~1125 μM for free TMZ in C6 glioma cells. Similarly, in U87MG cells, the Hybrid TMZ NCs showed an IC_{50} of ~866 μM compared to

~738 μM for free TMZ. This could be attributed due to the characteristic behaviour of the C6 and U87MG glioma cells. The C6-glioma cells are very aggressive in nature compared to the U87MG cells, which are comparatively less aggressive. It has been reported previously that, in C6 glioma cells, drug loaded nanoparticles have shown reduction in the cell viability compared to the free drug counterpart. On contrary, in U87MG glioma cells, a non-significant change in the growth rate was observed in drug loaded nanoparticles compared to the free drug treated group [26]. Likewise, previously, we have reported the cytotoxicity of TMZ in glioma cell lines with IC_{50} of >1,000 μM and ~700 μM in C6 and U87MG glioma cells, respectively [12]. Additionally, no major signs of reduction in cell viability were seen in both C6 and U87MG glioma cells post treatment with blank nanoparticles (without TMZ) with polymer concentration equivalent to Hybrid TMZ NCs (Fig. S7), indicating biocompatibility of polycarbonate-polyester based nanomaterials.

The cellular uptake of Hybrid TMZ nanoconjugate was analyzed in C6 and U87MG glioma cells using coumarin-6 as a fluorescent dye that showed an improved uptake in both glioma cells. Flow cytometry analysis also confirmed that the developed Hybrid TMZ NCs exhibited uptake efficiency of ~74 % and ~79 % in C6 and U87MG glioma cells, respectively (Fig. 6). Likewise, Pukale et al. prepared lipid-polymer hybrid nanoparticles for the delivery of clobetasol propionate for psoriasis like skin condition, wherein, LPNs with particle size of 94.8 nm exhibited improved cellular uptake up to 99.81 % with significantly improved *ex vivo* epidermis and dermis penetration into the psoriatic like skin [15]. Another study reported that the lipid-polymeric hybrid nanoparticles loaded with erlotinib and bevacizumab exhibited improved uptake efficiency of up to 52.3 % with reduced cellular viability compared to free drug treatment in A549 lung cancer cells [27]. Thereafter, endo-lysosomal fate of Hybrid TMZ NCs was determined using LysoTracker™ Red DND-99 as a fluorescent probe. Wherein, the confocal imaging analysis indicated that the Hybrid TMZ NCs exhibited the colocalization of the nanoconjugates in the endo-lysosomes with a colocalization index of 0.521 and 0.463 in C6 and U87MG glioma cells, respectively (Fig. 7).

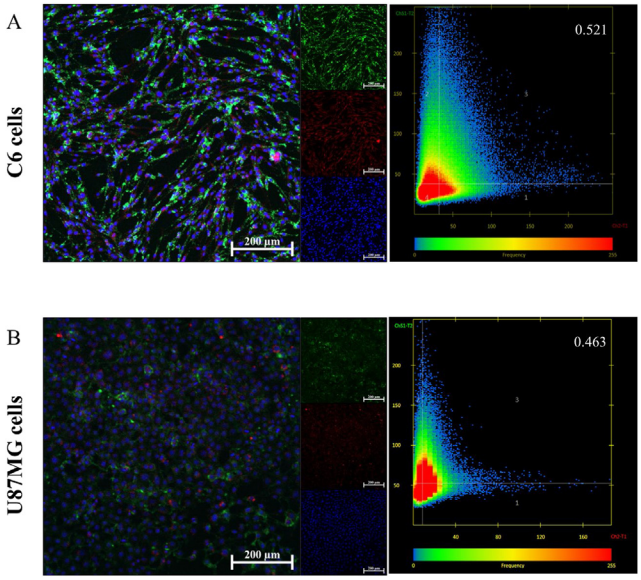

Fig. 7 – *In vitro* endo-lysosomal fate of Hybrid TMZ NCs in (A) C6 and (B) U87MG glioma cells.

3.6. *Apoptosis assay*

Apoptosis analysis was performed using the Annexin-V/PI staining method to determine the apoptosis in C6 and U87MG glioma cells after treatment with free TMZ and Hybrid TMZ NCs. Fig. 6 represents the apoptosis in C6 glioma cells, wherein the Hybrid TMZ NCs demonstrated significant improvement in apoptosis of 27.6 % (early apoptosis: 25.4 % and late apoptosis: 2.1 %) compared to free TMZ with apoptosis of 15.5 % (early apoptosis: 15.45 % and late apoptosis: 0.05 %). Similarly, in U87MG cells, the Hybrid TMZ NCs showed a significantly improved apoptosis of 42.75 % (early apoptosis: 40.99 % and late apoptosis: 1.76 %) compared to free TMZ with apoptosis of 21.33 % (early apoptosis: 20.57 % and late apoptosis: 0.76 %), indicating the improved efficacy of Hybrid TMZ NCs. Likewise, previously, we have reported the apoptosis of TMZ in glioma cell lines with total apoptosis of 18.28 % and 25.32 % in C6 and U87MG glioma cells, respectively [12].

3.7. *In vivo efficacy*

The *in vivo* antitumor efficacy of Hybrid TMZ NCs was evaluated in C6 cells-induced orthotropic syngeneic glioma model in *Sprague Dawley* rats. Animals were treated with free TMZ and Hybrid TMZ NCs at a dose equivalent to 10 mg/kg of TMZ thrice a week for 30 d, as reported in previous literature [12] (Fig. 8A). The positive control animals were treated with saline to nullify the placebo effect. The positive control animals exhibited 100 % mortality in 15 d after initiation of treatment, while the free TMZ-treated group showed mortality up to 40 % till Day 40 (post 30 d treatment). Surprisingly, no mortality was observed in the Hybrid TMZ NCs treated group till 40 d (Fig. 8G). A noticeable weight loss was observed in all the animals after the injection of cells in the orthotropic site. This is mainly observed due to the recovery from the intra-cranial surgery and C6-glioma cell implantation to the orthotropic site, causing a surgery-induced reduction in appetite and eventually resulting in weight loss. However, after 7 d of glioma implantation, all animals exhibited initiation in recovering body weight. Since the C6-glioma cells were injected, and tumor growth was observed at the cortical site of the frontal lobe, which is not responsible for food and hunger, eventually resulting in recovery in the body weight of animals [28]. The brain tissue of all animals was excised and evaluated for brain weight, and RH/LH ratio was examined to confirm tumor growth. It was observed that the positive control group showed significantly higher brain weight and RH/LH compared to the negative control group (normal animals). Free TMZ-treated animals showed a nominal reduction in brain weight and RH/LH compared to the positive control group. Likewise, a similar observation has been made previously that induction of C6 cells orthotropic glioma model results in elevation of RH/LH ratio and the presence of tumor cell growth in

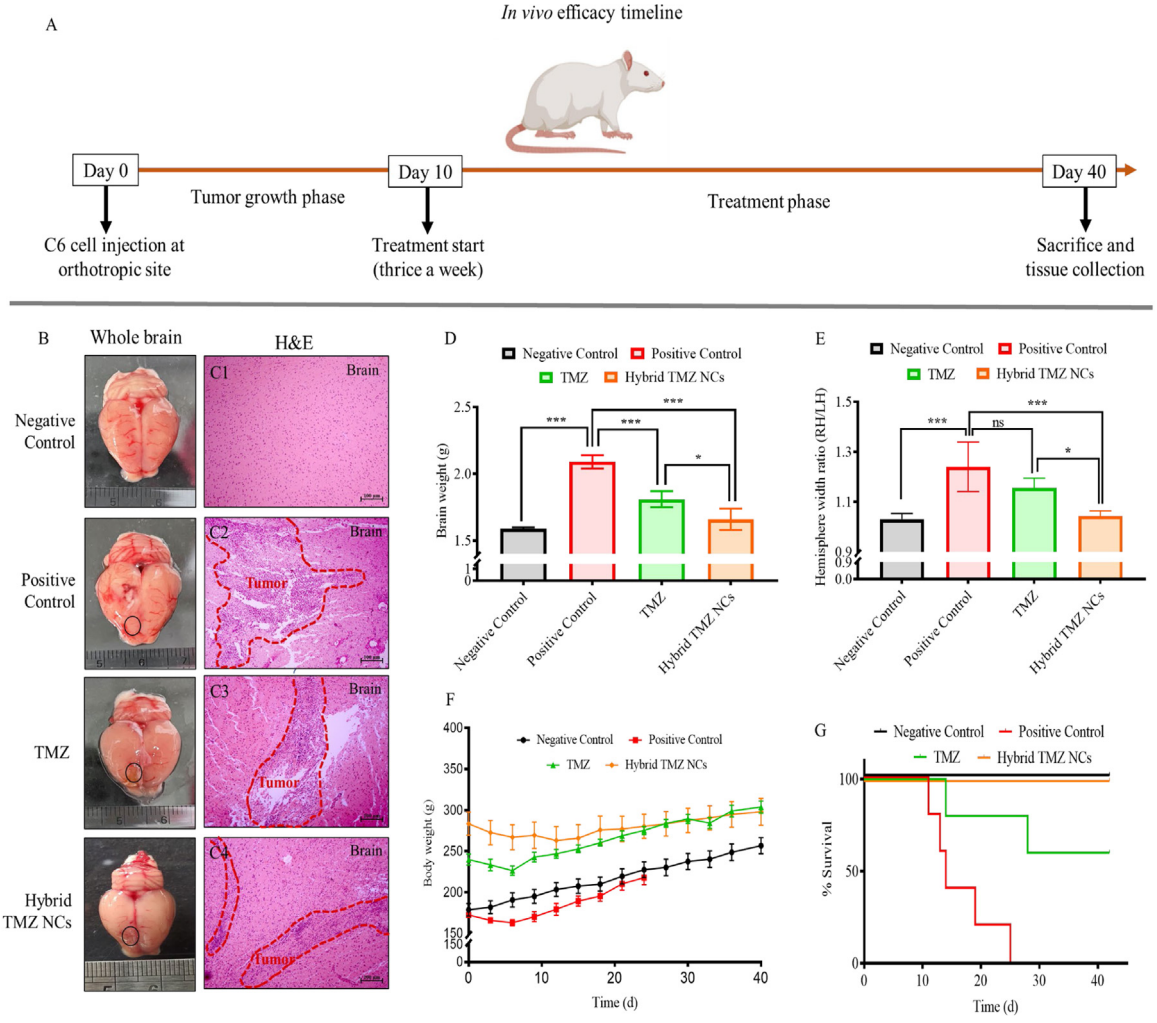

Fig. 8 – *In vivo* efficacy of hybrid nanoconjugates in C6 cells-induced orthotropic syngeneic glioma model in *Sprague Dawley* rats. (A) Treatment schedule. (B) Representative brain images of treatment groups (negative control, positive control, free TMZ-treated, and Hybrid TMZ NCs-treated) and its (C1-C4) brain histopathological (H&E) evaluation of the right hemisphere (at the site of injection). (D-G) represents mean brain weight, RH/LH ratio, body weight, and Kaplan-Meier survival plot of treated animals, respectively (scale bar: 100 µm) (*, * indicates *P* value <0.05, <0.001, respectively).**

the right hemisphere of the brain and metastatic cancer nodules in the lungs [12]. Further, treatment with Hybrid TMZ NCs demonstrated a statistically significant decrease in the brain weight and RH/LH ratio compared to the positive control group, indicating improved efficacy *in vivo* compared to the free TMZ-treated group (Fig. 8). Further, the excised brain was subjected to histopathological toxicity evaluation. Fig. 8 (C1-C4) shows the brain histopathological analysis of the positive control group with significantly higher infiltration of mononuclear cells/tumor cells at the site of injection (dotted line) depicting the tumor growth. In contrast, no such infiltration was observed in the left hemisphere of the brain, showing normal cellular morphology with no infiltration of C6 cells (uninjected site) *(data not shown)*. Treatment with Hybrid TMZ NCs showed a reduction in the mononuclear cells in the right hemisphere of the brain compared to the positive control group, indicating their effectiveness on the tumor burden in glioma-bearing rats.

3.8. *Toxicity evaluation of hybrid nanoconjugates*

The histopathological evaluation of various organs, including the heart, lungs, liver, kidney, and spleen, were evaluated using H&E staining to study the toxicity of the Hybrid TMZ NCs (Fig. 9). The negative control (healthy animals) depicted normal morphology of the heart tissue with central nuclei and syncytial arrangement of fibres with intercalated disks. Similarly, treatment groups (positive control, free TMZ and hybrid TMZ NCs) showed similar histology regarding fibre arrangement and the presence of intercalated discs. Lungs are considered to be highly perfused organ and become the primary target of cancer cells. The positive control group treated with saline showed moderate tumor cell infiltration to the lungs with an increased mitotic cell infiltration compared to the negative control group. Upon treatment with free TMZ, a slight reduction in infiltration was observed. Interestingly, treatment with Hybrid TMZ NCs demonstrated a significant

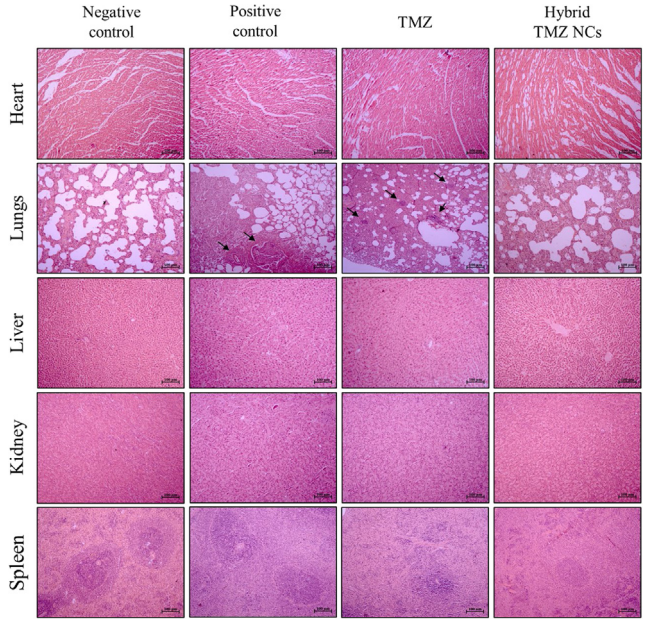

Fig. 9 – *In vivo* H&E evaluation of hybrid nanoconjugate in majorly excised organs (heart, lungs, liver, kidney, and spleen) in C6 cells-induced orthotopic glioma model in SD rats using H&E staining. (lungs: arrow indicates the presence of mitotic nucleus) (scale bar: 100 μm).

decrease in the mitotic nucleus and thickened alveolar septa, showing the positive anticancer outcome of the developed hybrid nanoconjugates on the lungs.

In histopathological analysis of the liver, the negative control group depicted the standard architecture of liver components consisting of hepatocytes, central vein, kupffer cells, bile duct cells, etc. In contrast, the positive control and TMZ-treated groups showed degenerative changes to the liver hepatocytes. In comparison, Hybrid TMZ NCs treated groups demonstrated the normal architecture of the liver components (hepatocytes, kupffer cells, bile duct cells). Further, kidneys of the positive control tumor-bearing animals depicted alteration in the kidney components, such as atrophic renal tubules with increased peritubular space, and a similar trend was observed in free TMZ-treated animals (Fig. 9). Treatment with Hybrid TMZ NCs yielded improved kidney histology with normal renal cortex, medulla, renal papilla, renal tubules, and glomerular tufts. The microscopic evaluation of splenic histology showed treatment with free TMZ, which showed moderate depletion in white pulp lymphoid components. At the same time, Hybrid TMZ NCs improved the splenic architecture with normal lymphoid follicles and sinuses with slight to minimal lymphoid depletion.

It is well known that polycarbonates have been used as biocompatible materials for improved mechanical support and delivery outcomes, giving desired therapeutic outcomes. Polycarbonates are composed of carbonate linkages that degrade slowly under physiological conditions and provide the controlled hydrolysis carbonate group, producing carbon dioxide and alcohol, thereby imparting the biocompatibility and biodegradability properties [29]. A similar observation has been seen by Rana et al., wherein no significant abnormalities were seen in major organs, including the brain, liver, heart, kidney, spleen, and lungs, and found to be safe post PEG-PLA administration [30]. Furthermore, He et al. prepared biodegradable polycarbonate micelles of mPEG-b-PMCC copolymer for the anticancer agent delivery, depicting good biocompatibility with blood and all the major tissues as no such toxicity was observed in histopathological evaluation [31]. Likewise, in the current study, we have utilized two different polymers, namely, polycarbonate-based and polyester-based copolymers. It has been earlier reported that both the polymers are biocompatible and biodegradable [31, 32], thus has minimal potential to cause any significant adverse effect on the organs.

Overall, the hybrid nanoconjugates approach exhibited better biocompatibility, improved the physiochemical and biological properties of the TMZ and recuperated organ components to normal levels with minimal to negligible toxicity comparable to the negative control group (Fig. 9).

4. Conclusion

Although TMZ is a potent chemotherapeutic for the treatment of GBM, still the therapeutic outcome is limited due to drug-related limitations. However, combining the conjugation with a hybrid nanocarrier approach has remarkably improved the loading capacity, stability half-life, and *in vitro* and *in vivo* efficacy. The hybrid nanoconjugates have enhanced cellular uptake, IC_{50} and apoptosis in C6 and U87MG glioma cells. *In vivo* administration has demonstrated improvement in the antitumor outcome compared to the free TMZ, with a significant improvement in the brain weight, hemispherical width ratio, and improved overall survival of rats. Histopathological evaluation has shown a reduction in the mononuclear cell infiltration in the brain tissue, and no other significant signs of toxicity were observed in the heart, liver, lungs, kidney and spleen, demonstrating the biocompatibility of the developed hybrid nanoconjugates. Thus, such a strategy could be explored for the delivery of drugs with disparate physiochemical properties to target the glioma.

Conflicts of interest

The authors declare that there is no conflicts of interest.

Acknowledgment

We acknowledge Department of Biotechnology, Government of India for the financial support to DC through a research grant (BT/PR22123/NNT/28/1120/2016). We thank Department of Science and Technology (DST) for their financial support through DST-INSPIRE fellowship to PS (DST/ INSPIRE Fellowship/ 2018/ IF180652)

Supplementary materials

Supplementary material associated with this article can be found, in the online version, at doi:10.1016/j.ajps.2025.101022.

REFERENCES

[1] Jatyan R, Singh P, Sahel DK, Karthik YG, Mittal A, Chitkara D. Polymeric and small molecule-conjugates of temozolomide as improved therapeutic agents for glioblastoma multiforme. J Control Release 2022;350:494–513.

[2] Nordling-David MM, Yaffe R, Guez D, Meirow H, Last D, Grad E, et al. Liposomal temozolomide drug delivery using convection enhanced delivery. J Control Release 2017;261:138–46.

[3] Duwa R, Banstola A, Emami F, Jeong JH, Lee S, Yook S. Cetuximab conjugated temozolomide-loaded poly (lactic-co-glycolic acid) nanoparticles for targeted nanomedicine in EGFR overexpressing cancer cells. J Drug Deliv Sci Technol 2020;60:101928.

[4] Audebert P, Clavier G, Allain C. Triazines, tetrazines, and fused ring polyaza systems. Prog Heterocycl Chem 2017;29:483–518.

[5] Du K, Xia Q, Heng H, Feng F. Temozolomide–doxorubicin conjugate as a double intercalating agent and delivery by apoferritin for glioblastoma chemotherapy. ACS Appl Mater Interfaces 2020;12:34599–609.

[6] Rai R, Banerjee M, Wong DH, McCullagh E, Gupta A, Tripathi S, et al. Temozolomide analogs with improved brain/plasma ratios – exploring the possibility of enhancing the therapeutic index of temozolomide. Bioorg Med Chem Lett 2016;26:5103–9.

[7] Park M, Song C, Yoon H, Choi K-H. Double blockade of glioma cell proliferation and migration by temozolomide conjugated with NPPB, a chloride channel blocker. ACS Chem Neurosci 2016;7:275–85.

[8] Cho HY, Swenson S, Thein TZ, Wang W, Wijeratne NR, Marín-Ramos NI, et al. Pharmacokinetic properties of the temozolomide perillyl alcohol conjugate (NEO212) in mice. Neuro-Oncology Adv 2020;2:vdaa160.

[9] Ward SM, Skinner M, Saha B, Emrick T. Polymer–temozolomide conjugates as therapeutics for treating glioblastoma. Mol Pharm 2018;15:5263–76.

[10] Patil R, Portilla-Arias J, Ding H, Inoue S, Konda B, Hu J, et al. Temozolomide delivery to tumor cells by a multifunctional nano vehicle based on poly(β-L-malic acid). Pharm Res 2010;27:2317–29.

[11] Xu K, Zhang L, Gu Y, Yang H, Du B, Liu H, et al. Increased the TMZ concentration in brain by poly(2-ethyl-2-oxazoline) conjugated temozolomide prodrug micelles for glioblastoma treatment. Eur Polym J 2021;145:110232.

[12] Jatyan R, Sahel DK, Singh P, Sakhuja R, Mittal A, Chitkara D. Temozolomide-fatty acid conjugates for glioblastoma multiforme: *in vitro* and *in vivo* evaluation. J Control Release 2023;61:161–74.

[13] Chitkara D, Mittal A, Behrman SW, Kumar N, Mahato RI. Self-assembling, amphiphilic polymer–gemcitabine conjugate shows enhanced antitumor efficacy against human pancreatic adenocarcinoma. Bioconjug Chem 2013;24:1161–73.

[14] Scopel R, Falcão MA, Cappellari AR, Morrone FB, Guterres SS, Cassel E, et al. Lipid-polymer hybrid nanoparticles as a targeted drug delivery system for melanoma treatment. Int J Polym Mater Polym Biomater 2022;71:127–38.

[15] Pukale SS, Sharma S, Dalela M, kumar Singh A, Mohanty S, Mittal A, et al. Multi-component clobetasol-loaded monolithic lipid-polymer hybrid nanoparticles ameliorate imiquimod-induced psoriasis-like skin inflammation in swiss albino mice. Acta Biomater 2020;115:393–409.

[16] Pukale SS, Sahel DK, Mittal A, Chitkara D. Coenzyme Q10 loaded lipid-polymer hybrid nanoparticles in gel for the treatment of psoriasis like skin condition. J Drug Deliv Sci Technol 2022;76:103672.

[17] Date T, Nimbalkar V, Kamat J, Mittal A, Mahato RI, Chitkara D. Lipid-polymer hybrid nanocarriers for delivering cancer therapeutics. J Control Release 2018;271:60–73.

[18] Sharma S, Mazumdar S, Italiya KS, Date T, Mahato RI, Mittal A, et al. Cholesterol and morpholine grafted cationic amphiphilic copolymers for miRNA-34a delivery. Mol Pharm 2018;15:2391–402.

[19] Sharma S, Pukale S, Sahel DK, Singh P, Mittal A, Chitkara D. Folate targeted hybrid lipo-polymeric nanoplexes containing docetaxel and miRNA-34a for breast cancer treatment. Mater Sci Eng C 2021;128:112305.

[20] Mittal A, Chitkara D, Behrman SW, Mahato RI. Efficacy of gemcitabine conjugated and miRNA-205 complexed micelles for treatment of advanced pancreatic cancer. Biomaterials 2014;35:7077–87.

[21] Ouellette RJ, Rawn JD. 20 - Carboxylic acids. In: Ouellette RJ, Rawn JDBT-OC, editors. Organic chemistry study guide. Boston: Elsevier; 2014. p. 659–98.

[22] Li Y, Wu H, Yang X, Jia M, Li Y, Huang Y, et al. Mitomycin C-soybean phosphatidylcholine complex-loaded self-assembled PEG-Lipid-PLA hybrid nanoparticles for targeted drug delivery and dual-controlled drug release. Mol Pharm 2014;11:2915–27.

[23] Tan S, Li X, Guo Y, Zhang Z. Lipid-enveloped hybrid nanoparticles for drug delivery. Nanoscale 2013;5:860–72.

[24] Tahir N, Madni A, Correia A, Rehman M, Balasubramanian V, Khan MM, et al. Lipid-polymer hybrid nanoparticles for controlled delivery of hydrophilic and lipophilic doxorubicin for breast cancer therapy. Int J Nanomedicine 2019;14:4961–74.

[25] Ebrahimian M, Mahvelati F, Malaekeh-Nikouei B, Hashemi E, Oroojalian F, Hashemi M. Bromelain loaded lipid-polymer hybrid nanoparticles for oral delivery: formulation and characterization. Appl Biochem Biotechnol 2022;194:3733–48.

[26] Xu Y, Shen M, Li Y, Sun Y, Teng Y, Wang Y, et al. The synergic antitumor effects of paclitaxel and temozolomide co-loaded in mPEG-PLGA nanoparticles on glioblastoma cells. Oncotarget 2016;7:20890.

[27] Pang J, Xing H, Sun Y, Feng S, Wang S. Non-small cell lung cancer combination therapy: hyaluronic acid modified, epidermal growth factor receptor targeted, pH sensitive lipid-polymer hybrid nanoparticles for the delivery of erlotinib plus bevacizumab. Biomed Pharmacother 2020;125:109861.

[28] Hirokawa J, Vaughan A, Masset P, Ott T, Kepecs A. Frontal cortex neuron types categorically encode single decision variables. Nature 2019;576:446–51.

[29] Ansari I, Singh P, Mittal A, Mahato RI, Chitkara D. 2,2-Bis(hydroxymethyl) propionic acid based cyclic carbonate monomers and their (co)polymers as advanced materials for biomedical applications. Biomaterials 2021;275:120953.

[30] Rana S, Singh J, Wadhawan A, Khanna A, Singh G, Chatterjee M. Evaluation of *in vivo* toxicity of novel biosurfactant from candida parapsilosis loaded in PLA-PEG polymeric nanoparticles. J Pharm Sci 2021;110:1727–38.

[31] He M, Wang R, Wan P, Wang H, Cheng Y, Miao P, et al. Biodegradable Ru-containing polycarbonate micelles for photoinduced anticancer multitherapeutic agent delivery and phototherapy enhancement. Biomacromolecules 2022;23:1733–44.